

Fermi surface mediated enhancement of bulk photovoltaic effects in ZnGeP₂

Banasree Sadhukhan^{1,2}

¹*Department of Physics and Nanotechnology, SRM Institute of Science and Technology, Kattankulathur, 603203, Chennai, Tamil Nadu, India**

²*Tata Institute of Fundamental Research, Hyderabad, Telangana 500046, India*

Bulk photovoltaic effect is a non-linear response in noncentrosymmetric materials that converts light to a DC current. In this work, we investigate the optical linear and non-linear responses of the chalcopyrite semiconductor ZnGeP₂. We report the enhancement of bulk photovoltaics namely shift and circular photogalvanic (CPG) current conductivities due to intrinsic contribution of Fermi surface along the high symmetry $\Gamma - Z$ direction. We observe that the magnification of shift and CPG current conductivities around the incident photon energy ~ 5 eV are about 38% and 81% respectively in ZnGeP₂ due to shifting of Fermi level to 1.52 eV. To further verify our findings, we explore distribution of bulk Fermi surface states in both three dimensional Brillouin zone and surface Fermi surface distribution in the projected energy landscape using semi infinite slab geometry. Our study not only provides a deeper understanding of the roles of Fermi surface contribution on the bulk photovoltaic responses, but also suggests the ZnGeP₂ is an ideal candidate for optoelectronics.

I. INTRODUCTION

Sustainable energy demands the development of new platforms for efficient solar energy conversion. The Shockley-Queisser limit constrains the performance of conventional solar cells based on p-n junctions, so alternative approaches are worth exploring. One of the most promising alternative sources of photocurrent is the bulk photovoltaic effect (BPVE) that produces photocurrents in materials lacking inversion symmetry and unlike conventional p-n junctions, the generated photovoltage is above the bandgap limit [1, 2]. BPVE is a second-order nonlinear response, which can be decomposed into a linear photogalvanic effect (LPGE) and a circular photogalvanic effect (CPGE), respectively, based on the linear and circular polarization state of the incident light respectively [1–12]. The CPGE can be directly related to the Berry curvature of the Bloch bands involved in the optical transition and proportional to the topological charge of the Weyl semimetals [12]. Microscopically, the shift current (LPGE) originates from the shift of the wave packet of Bloch electrons during interband photoexcitation [11].

Nonlinear responses are creating new opportunities for revealing the topology and band structure geometry in condensed matter systems [9, 13, 14]. For example, shift and circular photocurrents, nonlinear susceptibilities are being explored as probes of the details of the crystallographic orientation, band structure geometry, grain boundaries [3, 10, 11, 15–18], Hall effects in both time-reversal invariant and broken systems [19–22]. The effects of the Fermi surface and disorder on nonlinear optical response have started to gain attention very recently [20, 23–30]. Intrinsic contribution of Fermi surface to the BPVE has been reported in metallic systems under illumination by polarized light [24, 25]. Interplay between

band geometric quantities give rises to the second harmonic generation which produces resonant peaks in optical response for topological materials due the Fermi surface [26–29]. Recent studies have shown that subbandgap photocurrents due to band broadening in semiconductors and insulators can be used to measure finite lifetimes, in contrast to clean limit [30].

The fundamental requirement for a material to produce a current via the BPVE is the broken inversion symmetry which allows the asymmetric photoexcitation of charge carriers induced by electron-phonon or electron-electron scattering. BPVE has recently drawn attention in class of materials like hybrid perovskites, polar topological insulators, Weyl semimetals [6, 10, 31–33]. Chalcopyrite semiconductors have drawn attention for its potential application as a nonlinear optical material [8, 34]. ZnGeP₂ is a one of the chalcopyrite semiconductor is thought to be derived from zinc-blende III-V parent compound GaP by replacing pairs of neighboring group-III elements Ga by a group II-Zn or group IV-Ge atoms. In chalcopyrite structures, c/a ration is slightly lower than 2 which produces a compressive uniaxial strain and effects on the Brillouin zone (BZ) of zinc-blende structures. The conduction-band minimum of the mother structure of GaP at X point in the BZ is folded onto the Γ point of the ZnGeP₂ [35]. Therefore, Γ point in the BZ has a strong impact on optical response of chalcopyrite compounds [35–40]. A model was proposed based on the splittings of the low-lying conduction-band states at Γ point in order to explain the strong peak in the photoluminescence spectra [36–38]. Controlled doping of Sc atoms in ZnGeP₂ move the Fermi level upward to 0.8 eV [41].

In this work, we study the optical linear and non-linear response for a chalcopyrite semiconductor ZnGeP₂. Using extensive first-principles-based calculations, we report the enhancement of bulk photovoltaics like shift and CPG current conductivities due to intrinsic contribution of Fermi surface states around $\Gamma - Z$ direction in the BZ. We found that the inclusion of Fermi surface effect can

* banasres@srmist.edu.in

significantly improve the generation of bulk photovoltaics responses. Especially, we predict that enhancement are 38% and 81% respectively for shift and CPG current conductivities due to shifting of Fermi level to 1.52 eV around the peak of responses. The distribution of bulk Fermi surface states in the projected energy landscape is also explored using semi-infinite slab geometry to examine microscopically the contribution Fermi surface states in the BZ on the enhancement of BPVE. The paper is organised as follows. In Sec. II we describe the computational details. In Sec. III we discuss our results on both linear and non-linear responses along with the electronic structure and enhancement of BPVE in ZnGeP₂. Finally in Sec. IV, we conclude with future perspectives.

II. COMPUTATIONAL DETAILS

Chalcopyrite semiconductors crystallize into the tetragonal structure with a space group $I\bar{4}2d$. The atomic positions of ZnGeP₂ are Zn (0, 0, 0), Ge (0, 0, 0.5) and P (u, 0.25, 0.125), where u is the internal displacement parameter for the anion. The anion acquires an equilibrium position closer to one pair of cations as a result of dissimilar atoms as neighbors. The structural relaxation are done in Vienna Ab initio Simulation Package (VASP) with kpoints $12 \times 12 \times 12$ [42, 43]. The optimized lattice constants (a and c) and the internal structural parameter (u) are $a = 5.454 \text{ \AA}$, $c = 10.707 \text{ \AA}$ and $u = 0.267 \text{ \AA}$ respectively. The density functional theoretical calculations are performed using the local density approximation (LDA) method as implemented within full-potential local-orbital (FPLO) code [44].

In the next step, we use a tight-binding model with the Wannier function basis to calculate the shift and CPG current conductivities. The tight-binding model is obtained using maximally projected Wannier functions for the Zn-3d, 4s, Ge-3d, 4s, 4p and P-3s, 3p orbitals in the energy range of -9.0 to 5.0 eV. BZ was sampled by a $150 \times 150 \times 150$ kpoints with satisfactory convergence. This Wannier model is used to calculate the spectral density for an infinite bulk system by k_z -integrating bulk projected band structure. Furthermore, a semi-infinite slab is set up to calculate spectral densities of [001]-surface. The spectral densities for both bulk and semi-infinite slab geometry are obtained using Green's function recursion method [45].

III. RESULTS AND DISCUSSION

A. Electronic structure

Figure 1 (a) represent the band structure along the high symmetry directions for ZnGeP₂ respectively. There is a remaining open question about the nature of its band gap whether it is direct, indirect or pseudo-direct because different studies lead to different results [35, 46–

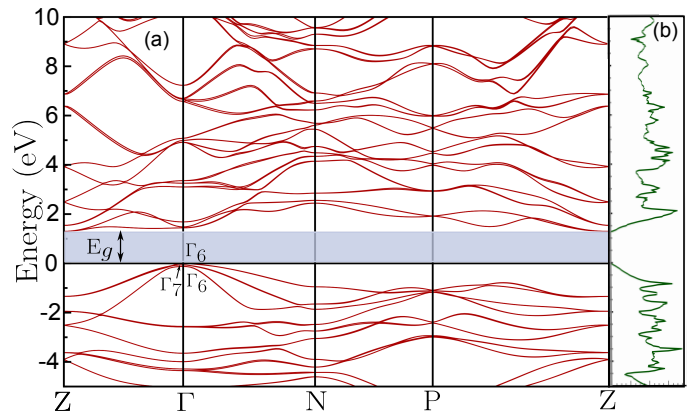


FIG. 1. (a) Band structure and (b) total density of states for ZnGeP₂.

49]. The top of the valence band locates at Γ point and the bottom of the conduction band minimum locates at Z point. Therefore ZnGeP₂ has a indirect band gap of 1.32 eV from LSDA calculations. In comparing the with the experimental data, the calculated band gap is underestimated. It is obvious that the band gap calculated by DFT is smaller than the one measured experimentally. This error can be explained by the discontinuity of different exchange-correlation potentials. Without spin-orbit coupling, triply degenerated Γ_{15} valence band of its III-V zinc-blende compounds splits into a non-degenerate bands of Γ_4 and Γ_5 resulting a finite crystal field splitting ($\Delta_{cf} = E(\Gamma_5) - E(\Gamma_4)$) in chalcopyrite structures. In presence of spin-orbit interactions, Γ_5 splits into Γ_6 , Γ_7 and $\Gamma_4 \rightarrow \Gamma_6$ resulting $\Delta_{cf} = E(\Gamma_7) - E(\Gamma_6)$ [35, 50]. When the anion position parameter u of chalcopyrite crystal deviates from 0.25, the absolute value of crystal field splitting increases. This is because the chalcopyrite materials deform compared to its parent zincblende structures. Therefore Δ_{cf} is zero in GaP, whereas it is of -102.5 meV for ZnGeP₂.

To get more insight into the the electronic structure, we look into the total (see Fig. 1(b)) and partial (see Fig. 4 in appendix) density of states of ZnGeP₂. The low-energy valence bands are mainly due to P-3p state with an admixture of Ge-4p and Zn-4p states, whereas Ge-4s, P-3d and Zn-4d states are also contributing to conduction band in addition to them. By analyzing the partial density states, one can clearly observed the strong effects of p-d hybridization which modifies the energy gap. The p-like states are pushed up and Zn-d like states are pushed down generating a band gap 1.32 eV for ZnGeP₂

B. Linear optical response

The optical properties of ZnGeP₂ can be calculated from the complex dielectric function. In the presence of an electric field, the complex dielectric function can be divided into two parts: the intraband transition and

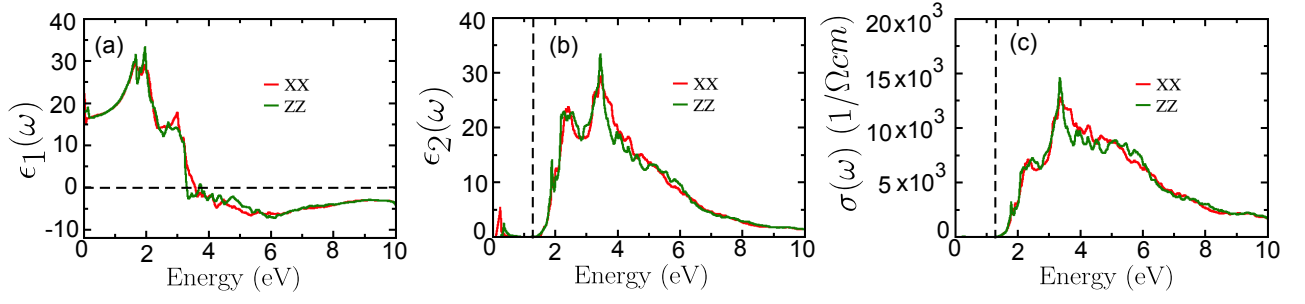


FIG. 2. (a) The real and (b) imaginary parts of the dielectric constant, and (c) optical conductivity as a function of the incident photon energy.

the interband transition. In the case of metals, intraband transitions are useful, while in the case of semiconductors, interband transitions are useful. Interband transitions can be of two types: direct band transitions and indirect band transitions. Since the indirect interband transition contributes little to the dielectric function, which involves electron-phonon scattering, it can be ignored. By calculating the momentum matrix elements between occupied and unoccupied wave functions, the direct interband contribution can be calculated.

The optical properties within the linear response theory are obtained from the imaginary part of the dielectric function, which is given by

$$\epsilon_2^{ij}(\omega) = \text{Im}[\epsilon_{ij}(\omega)] = -\frac{4\pi^2 e^2}{m_0^2 \omega^2} \int dk \sum_{n,l} (f_n - f_l) \times \frac{\langle \vec{k}n | \hat{v}_i | \vec{k}l \rangle \langle \vec{k}l | \hat{v}_j | \vec{k}n \rangle}{(E_{\vec{k}n} - E_{\vec{k}l} - \hbar\omega - i\delta)}, \quad (1)$$

where, $i, j = (x, y, z)$ are the Cartesian coordinates, $\hat{v}_i = \hat{p}_i/m_0$, m_0 is the free electron mass, $|\vec{k}n\rangle$ are the wavefunctions corresponding to the band with energy $E_{\vec{k}n}$ at momentum \vec{k} and index n , $f_n \equiv f(E_{\vec{k}n})$ is the Fermi function for the state with energy $E_{\vec{k}n}$, and $\hbar\omega$ is the incident photon energy. $\delta = \hbar/\tau_s$ is the broadening parameter and depends inversely on the single-particle relaxation time associated with the quantum mechanical broadening τ_s . The real part of the dielectric function can be obtained via the Kramer-Kronig relation:

$$\epsilon_1^{ij}(\omega) = \text{Re}[\epsilon_{ij}(\omega)] = \delta_{ij} + \frac{1}{\pi} \mathcal{P} \int_{-\infty}^{\infty} d\omega' \frac{\text{Im}[\epsilon_{ij}(\omega')]}{\omega - \omega'}. \quad (2)$$

The optical conductivity is given by:

$$\sigma_{ij}(\omega) = \frac{\omega \epsilon_2^{ij}(\omega)}{4\pi}. \quad (3)$$

Figure 2(a)-(b) represent the real and imaginary parts of the dielectric function. $\epsilon_1(\omega)$ has a peak with a magnitude of 33.02 at around 1.98 eV. It then sharply decreases between 1.98 eV and 3.36 eV and becomes negative after that. The minimum of $\epsilon_1(\omega)$ occurs at 6.02 eV followed

by a slow increase toward zero. The static dielectric constant $\epsilon_1(0) = 18.01$ for ZnGeP₂. $\epsilon_2(\omega)$ shows that the threshold energy of the dielectric function occurs at 1.32 eV, i.e., above the band gap. The imaginary part of the dielectric constant $\epsilon_2(\omega)$ shows peaks at 2.41 and 3.44 eV, respectively. The small contributions of $\epsilon_2(\omega)$ below the band gap are coming from intraband transitions of the optical response. The calculated linear optical conductivities are presented in Fig. 2(c). It shows that optical transitions from valence to conduction bands occur above the band gap. $\sigma(\omega)$ produces a strong peak at 3.34 eV, followed by a weak peak at 2.32 eV, as shown in Fig. 2(c).

C. Bulk photovoltaics and effect of Fermi surface

For the bulk photovoltaic responses, the photoconductivity in quadratic response theory appears as [6, 8, 51, 52]:

$$\sigma_{ij}^k = \frac{|e|^3}{8\pi^3 \omega^2} \text{Re} \left\{ \phi_{ij} \sum_{\Omega=\pm\omega} \sum_{l,m,n} \int_{BZ} dk (f_l - f_n) \times \frac{\langle \vec{k}n | \hat{v}_i | \vec{k}l \rangle \langle \vec{k}l | \hat{v}_j | \vec{k}m \rangle \langle \vec{k}m | \hat{v}_k | \vec{k}n \rangle}{(E_{\vec{k}n} - E_{\vec{k}m} - i\delta)(E_{\vec{k}n} - E_{\vec{k}l} + \hbar\Omega - i\delta)} \right\}. \quad (4)$$

The conductivity σ_{ij}^k ($i, j, k = x, y, z$) is a third-rank tensor representing the photocurrent J_k generated by an electrical field via $J_k = \sigma_{ij}^k \mathcal{E}_i^* \mathcal{E}_j$. ϕ_{ij} is the phase difference between the driving field \mathcal{E}_i and \mathcal{E}_j . The real (imaginary) part of the integral in Eq. (4) describes the shift and CPG current conductivity under linearly and circularly polarized light, respectively.

Now we study the non-linear photocurrent responses under linearly and circularly polarized light, respectively, for different chemical potentials (3). As the photocurrent response arises from both real and virtual band transitions, it is generally strongly dependent on the incident photon energy. As we consider the relaxation time approximation, therefore we used $\delta = 10$ meV in our calculations. The current responses are along the x-direction for yz-polarization of light. Here both the non-linear photo-current conductivities are forbidden below

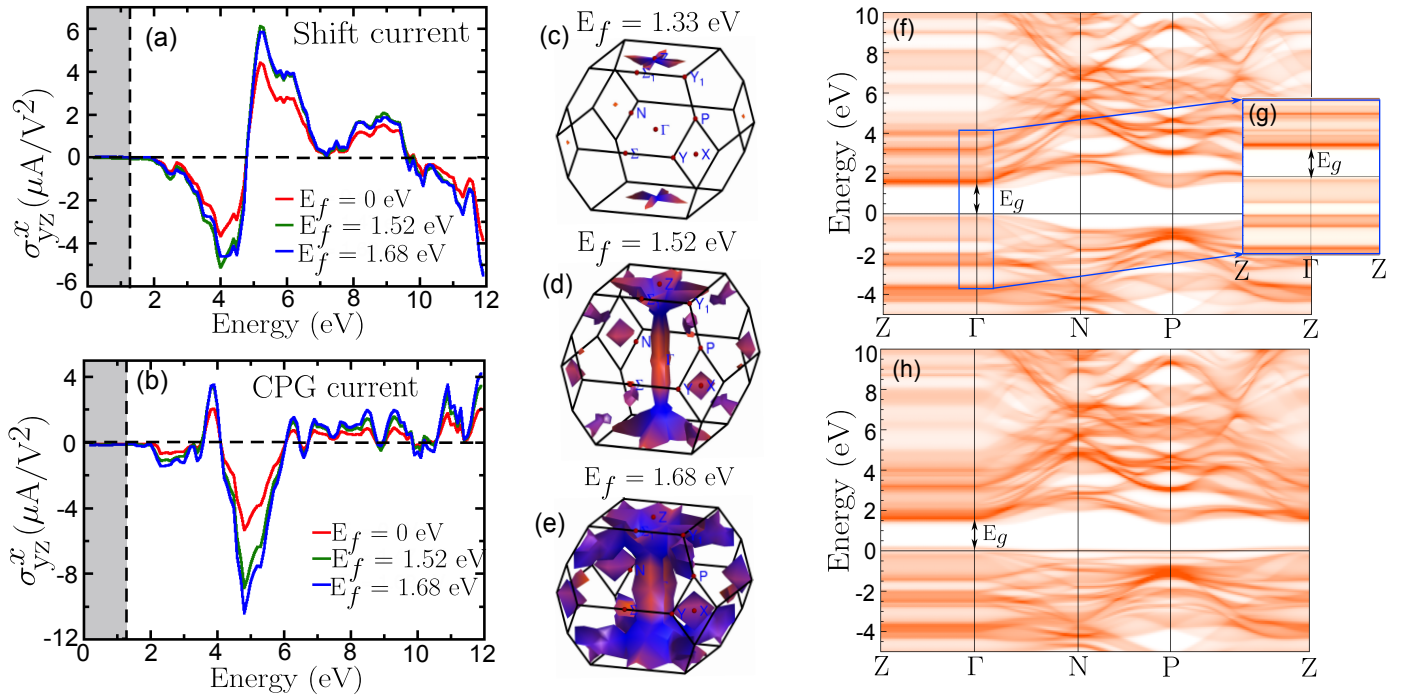


FIG. 3. Fermi surface mediated enhancement of bulk photovoltaic effects for (a) shift current conductivity and (b) CPG current conductivity with different chemical potentials E_f . (c)-(e) The bulk Fermi surface states in full Brillouin zone indicating high symmetry points for different chemicals E_f . (f)-(g) k_z -integrated [(001)-direction] bulk projected bands. (h) Energy distribution curve for [001]-surface in semi infinite slab.

the band i.e 1.32 eV. The peak of non-linear responses appear a few eV above the band gap but well outside the visible energy window.

Figure 3(a) presents the calculated shift current conductivity under linear polarization of light for different Fermi energies E_f . The shift current conductivity get a value of $-3.75 \mu\text{A}/\text{V}^2$ at the incident photo energy of ~ 4 eV when the chemical potential is at 0 eV. By shifting the Fermi level to $E_f = 1.52$ eV, σ_{yz}^x reaches to a value to $-5.19 \mu\text{A}/\text{V}^2$. Further shifting of Fermi energy $E_f = 1.68$ eV, slightly drop down to $-4.59 \mu\text{A}/\text{V}^2$. The shift current conductivity gets inverted above the incident energy of 4.8 eV and reaches to a peak value of $4.46 \mu\text{A}/\text{V}^2$ with $E_f = 0$ eV. However, the σ_{yz}^x enhances to 6.17 and $5.82 \mu\text{A}/\text{V}^2$ for $E_f = 1.52$ eV and 1.68 eV respectively. The shift current conductivity has positive magnitude for the incident energy windows of (4.8-9.7) eV and gets inverted otherwise and these nature of the responses are same for all chemical potentials as shown in Fig. 3(a). But the contributions to responses can vary significantly across the BZ for a given chemical potential E_f .

Figure 3(b) shows the calculated CPG current conductivity for different Fermi energies E_f . The CPG current conductivity at incident photo energies near the band gap is small. It reaches a maximum value of $-1.51 \mu\text{A}/\text{V}^2$ at 2.32 eV within visible energy spectrum. CPG current conductivity is negative just above band gap and reverses its direction resulting in a peak of $2.35 \mu\text{A}/\text{V}^2$ at 3.8 eV

followed by a broad peak of $-5.49 \mu\text{A}/\text{V}^2$ at 4.8 eV for Fermi energy $E_f = 0$ eV. Shifting chemical potential has a large effects also on CPG current conductivity. However, the CPG current conductivity reaches to -9.95 and $-10.76 \mu\text{A}/\text{V}^2$ at incident photon energy of 4.8 eV for $E_f = 1.52$ eV and 1.68 eV respectively.

Fermi surface has an intrinsic contribution to BPVE [24]. Both the shift and CPG current conductivities enhance by shifting the Fermi level above band gap to (1.52 - 1.68) eV as shown in Fig.3(a)-(b). To investigate the connection of photovoltaic effect to Fermi surface of ZnGeP_2 , we study the three dimensional (3D) bulk Fermi surface at different chemical potentials in the whole BZ. Figure 5(a)-(h) (in appendix) present the systematic evolution of the bulk 3D Fermi surface along with the high symmetry points in BZ by changing the chemical potential E_f from 1.33 to 2.15 eV above the band gap.

When the chemical potential touches at the conduction band just above the band gap ($E_f = 1.33$ eV), the contribution of the Fermi surface appears at high symmetry Z point as shown Fig.3(c). Further shifting of the chemical potential to $E_f = 1.52$ eV, the bulk 3D Fermi surface appears along the high symmetry line $\Gamma - Z$ directions instead of a small contribution only at Z point as shown in Fig. 3(d). The appearance of the bulk 3D Fermi surface broadens at the chemical potential $E_f = 1.68$ eV (see Fig. 3(e)). This enhances the both the shift and CPG current conductivities when the chemical potential are between (1.52 - 1.68) eV for ZnGeP_2 due to

Fermi surface states contribution along $\Gamma - Z$ direction to non-linear photocurrent. If we further move the chemical potential above $E_f = 1.68$ eV, the contribution of the bulk 3D Fermi surface in the BZ decreases along $\Gamma - Z$ direction (see 5 (e)-(h) in appendix) which results again decrease of both shift and CPG current conductivities in ZnGeP_2 .

To investigate further, we also study Fermi surface states contribution in the projected energy landscape instead of only in momentum space BZ landscape. Figure 3(f)-(g) and (h) present the k_z -integrated projected band in bulk and semi-infinite geometry respectively. The surface Fermi surface states available along $Z \leftarrow \Gamma \rightarrow Z$ direction at chemical potential around $E_f = 1.52$ eV above the band gap is due to the projection of bulk 3D Fermi surface (see Fig. 3 (d)-(e)) which contributes in the enhancement of BPVE in ZnGeP_2 . However, these states decrease after $E_f = 1.7$ eV.

IV. CONCLUSION

Chalcopyrite semiconductors provide a promising platform for observing bulk photovoltaics responses in addition to the linear response. We study the intrinsic Fermi surface contribution to nonlinear DC photocurrent, namely shift and CPG current. We find that the polarized light induces electronic transitions on the Fermi

surface that contribute to the enhancement of BPVE in ZnGeP_2 . The shift current and CPG current conductivities are 4.46 and -5.49 $\mu\text{A}/\text{V}^2$ with the incident photo energy at 4.8 eV for the chemical potential $E_f = 0$ eV which produces conductivities of 6.17 and -9.95 $\mu\text{A}/\text{V}^2$ respectively by shifting the chemical potentials to $E_f = 1.52$ eV. We report the enhancement of shift and CPG current conductivities are about 38% and 81% due to intrinsic Fermi surface states along the high symmetry $\Gamma - Z$ direction.

Our study is further collaborated by searching the Fermi surface states contribution in both momentum (3D BZ) and energy distribution landscape which produces intrinsic contribution to BPVE. In addition to non-linear responses, we also study the linear optical responses in ZnGeP_2 . Optical conductivity produces a peak of $14.83 \times 10^3 \Omega \cdot \text{cm}^{-1}$ at the incident photo energy of 3.35 eV. Relying on these in-depth understandings of the role of intrinsic Fermi surface effects and the prediction of enhancement of BPVE, ZnGeP_2 appears as a promising candidate for optoelectronic applications based on bulk photovoltaics. We believe that the results in our work will serve as a guide for both theory and experiment in the development and optimization of the next generation bulk photovoltaics in chalcopyrite materials [8].

V. ACKNOWLEDGEMENT

We acknowledge IFW Dresden cluster and Ulrike Nitzsche for technical support.

-
- [1] Subhajit Pal, S Muthukrishnan, Banasree Sadhukhan, Sarath NV, D Murali, and Pattukkannu Murugavel, "Bulk photovoltaic effect in batio3-based ferroelectric oxides: An experimental and theoretical study," *Journal of Applied Physics* **129** (2021).
 - [2] F. Nastos and J. E. Sipe, "Optical rectification and shift currents in gaas and gap response: Below and above the band gap," *Phys. Rev. B* **74**, 035201 (2006).
 - [3] J. E. Sipe and A. I. Shkrebtii, "Second-order optical response in semiconductors," *Phys. Rev. B* **61**, 5337-5352 (2000).
 - [4] Takahiro Morimoto and Naoto Nagaosa, "Topological aspects of nonlinear excitonic processes in noncentrosymmetric crystals," *Phys. Rev. B* **94**, 035117 (2016).
 - [5] F. Nastos and J. E. Sipe, "Optical rectification and current injection in unbiased semiconductors," *Phys. Rev. B* **82**, 235204 (2010).
 - [6] Yang Zhang, Hiroaki Ishizuka, Jeroen van den Brink, Claudia Felser, Binghai Yan, and Naoto Nagaosa, "Photogalvanic effect in weyl semimetals from first principles," *Phys. Rev. B* **97**, 241118 (2018).
 - [7] Banasree Sadhukhan and Tanay Nag, "Role of time reversal symmetry and tilting in circular photogalvanic responses," *Phys. Rev. B* **103**, 144308 (2021).
 - [8] Banasree Sadhukhan, Yang Zhang, Rajyavardhan Ray, and Jeroen van den Brink, "First-principles calculation of shift current in chalcopyrite semiconductor znsp_2 ," *Phys. Rev. Mater.* **4**, 064602 (2020).
 - [9] Banasree Sadhukhan and Tanay Nag, "Electronic structure and unconventional nonlinear response in double weyl semimetal Srsi_2 ," *Phys. Rev. B* **104**, 245122 (2021).
 - [10] Steve M. Young and Andrew M. Rappe, "First principles calculation of the shift current photovoltaic effect in ferroelectrics," *Phys. Rev. Lett.* **109**, 116601 (2012).
 - [11] Takahiro Morimoto and Naoto Nagaosa, "Topological nature of nonlinear optical effects in solids," *Science Advances* **2**, e1501524 (2016).
 - [12] Fernando de Juan, Adolfo G. Grushin, Takahiro Morimoto, and Joel E. Moore, "Quantized circular photogalvanic effect in weyl semimetals," *Nature Communications* **8**, 15995 (2017).
 - [13] J. Orenstein, J. E. Moore, T. Morimoto, D. H. Torchinsky, J. W. Harter, and D. Hsieh, "Topology and symmetry of quantum materials via nonlinear optical responses," *Annual Review of Condensed Matter Physics* **12**, 247-272 (2021).
 - [14] E. J. König, M. Dzero, A. Levchenko, and D. A. Pesin, "Gyrotropic hall effect in berry-curved materials," *Phys. Rev. B* **99**, 155404 (2019).
 - [15] Steve M. Young, Fan Zheng, and Andrew M. Rappe, "First-principles calculation of the bulk photovoltaic effect in bismuth ferrite," *Phys. Rev. Lett.* **109**, 236601 (2012).
 - [16] Ashley M. Cook, Benjamin M. Fregoso, Fernando de Juan, Sinisa Coh, and Joel E. Moore, "Design principles for shift current photovoltaics," *Nature Communi-*

- cations **8**, 14176 (2017).
- [17] Bruno R. Carvalho, Yuanxi Wang, Kazunori Fujisawa, Tianyi Zhang, Ethan Kahn, Ismail Bilgin, Pulickel M. Ajayan, Ana M. de Paula, Marcos A. Pimenta, Swastik Kar, Vincent H. Crespi, Mauricio Terrones, and Leandro M. Malard, “Nonlinear dark-field imaging of one-dimensional defects in monolayer dichalcogenides,” *Nano Letters* **20**, 284–291 (2020).
- [18] Xiaobo Yin, Ziliang Ye, Daniel A. Chenet, Yu Ye, Kevin O’Brien, James C. Hone, and Xiang Zhang, “Edge nonlinear optics on a mos2 atomic monolayer,” *Science* **344**, 488–490 (2014).
- [19] Pankaj Bhalla, Ming-Xun Deng, Rui-Qiang Wang, Lan Wang, and Dimitrie Culcer, “Nonlinear ballistic response of quantum spin hall edge states,” *Phys. Rev. Lett.* **127**, 206801 (2021).
- [20] Z. Z. Du, C. M. Wang, Shuai Li, Hai-Zhou Lu, and X. C. Xie, “Disorder-induced nonlinear hall effect with time-reversal symmetry,” *Nature Communications* **10**, 3047 (2019).
- [21] S. Nandy and Inti Sodemann, “Symmetry and quantum kinetics of the nonlinear hall effect,” *Phys. Rev. B* **100**, 195117 (2019).
- [22] Banasree Sadhukhan and Tanay Nag, “Effect of chirality imbalance on hall transport of prrh₂,” *Phys. Rev. B* **107**, L081110 (2023).
- [23] Jorge I. Facio, Dmitri Efremov, Klaus Koepernik, Jih-Shih You, Inti Sodemann, and Jeroen van den Brink, “Strongly enhanced berry dipole at topological phase transitions in bitei,” *Phys. Rev. Lett.* **121**, 246403 (2018).
- [24] Lingyuan Gao, Zachariah Addison, E. J. Mele, and Andrew M. Rappe, “Intrinsic fermi-surface contribution to the bulk photovoltaic effect,” *Phys. Rev. Res.* **3**, L042032 (2021).
- [25] Zaiyao Fei, Wenjin Zhao, Tauno A. Palomaki, Bosong Sun, Moira K. Miller, Zhiying Zhao, Jiaqiang Yan, Xiaodong Xu, and David H. Cobden, “Ferroelectric switching of a two-dimensional metal,” *Nature* **560**, 336–339 (2018).
- [26] G. Lefkidis and W. Hübner, “Phononic effects and non-locality contributions to second harmonic generation in nio,” *Phys. Rev. B* **74**, 155106 (2006).
- [27] Zhi Li, Ya-Qin Jin, Takami Tohyama, Toshiaki Iitaka, Jiu-Xing Zhang, and Haibin Su, “Second harmonic generation in the weyl semimetal taas from a quantum kinetic equation,” *Phys. Rev. B* **97**, 085201 (2018).
- [28] Pankaj Bhalla, Kamal Das, Dimitrie Culcer, and Amit Agarwal, “Resonant second-harmonic generation as a probe of quantum geometry,” *Phys. Rev. Lett.* **129**, 227401 (2022).
- [29] Pankaj Bhalla, Allan H. MacDonald, and Dimitrie Culcer, “Resonant photovoltaic effect in doped magnetic semiconductors,” *Phys. Rev. Lett.* **124**, 087402 (2020).
- [30] Daniel Kaplan, Tobias Holder, and Binghai Yan, “Nonvanishing subgap photocurrent as a probe of lifetime effects,” *Phys. Rev. Lett.* **125**, 227401 (2020).
- [31] Liang Z. Tan and Andrew M. Rappe, “Enhancement of the bulk photovoltaic effect in topological insulators,” *Phys. Rev. Lett.* **116**, 237402 (2016).
- [32] Kun Woo Kim, Takahiro Morimoto, and Naoto Nagaosa, “Shift charge and spin photocurrents in dirac surface states of topological insulator,” *Phys. Rev. B* **95**, 035134 (2017).
- [33] Xiao Jiang, Liangting Ye, Xiaoqiang Wu, Lei Kang, and Bing Huang, “Role of large rashba spin-orbit coupling in second-order nonlinear optical effects of polar bib₃o₆,” *Phys. Rev. B* **106**, 195126 (2022).
- [34] Surasree Sadhukhan, Banasree Sadhukhan, and Sudipta Kanungo, “Pressure-driven tunable properties of the small-gap chalcopyrite topological quantum material zn₂gesb₂: A first-principles study,” *Phys. Rev. B* **106**, 125112 (2022).
- [35] Sukit Limpijumnong, Walter R. L. Lambrecht, and Benjamin Segall, “Electronic structure of zngep₂: a detailed study of the band structure near the fundamental gap and its associated parameters,” *Phys. Rev. B* **60**, 8087–8096 (1999).
- [36] Yurri V. Rud, Vasilii Yu, M. C. Ohmer, and P. G. Shunemann, “Photoluminescence study of p-zn₂gep₂ crystals,” *MRS Online Proceedings Library* **450**, 339–344 (1996).
- [37] MC Petcu, NC Giles, PG Schunemann, and TM Polak, “Band-edge photoluminescence at room temperature from zngep₂ and ag₂ge₂,” *physica status solidi (b)* **198**, 881–888 (1996).
- [38] JE McCrae Jr, MR Gregg, RL Hengehold, YK Yeo, PH Ostdiek, MC Ohmer, PG Schunemann, and TM Polak, “Polarized luminescence study of ordered nonlinear optical material zngep₂,” *Applied physics letters* **64**, 3142–3144 (1994).
- [39] Guy Fishman and Bernard Sermage, “Structure of the *d* level and the *p* – *d* coupling in i-iii-v₂ chalcopyrite compounds,” *Phys. Rev. B* **18**, 7099–7103 (1978).
- [40] J. E. Jaffe and Alex Zunger, “Electronic structure of the ternary pnictide semiconductors zn₂sp₂, zngep₂, zn₂sn₂, zn₂si₂, and mgsip₂,” *Phys. Rev. B* **30**, 741–756 (1984).
- [41] Vladimir I Voevodin, Valentin N Brudnyi, Yury S Sarkisov, Xinyang Su, and Sergey Yu Sarkisov, “Electrical relaxation and transport properties of zngep₂ and 4h-sic crystals measured with terahertz spectroscopy,” in *Photonics*, Vol. 10 (MDPI, 2023) p. 827.
- [42] G. Kresse and J. Furthmüller, “Efficient iterative schemes for ab initio total-energy calculations using a plane-wave basis set,” *Phys. Rev. B* **54**, 11169–11186 (1996).
- [43] G. Kresse and J. Hafner, “Ab initio molecular dynamics for liquid metals,” *Phys. Rev. B* **47**, 558–561 (1993).
- [44] Klaus Koepernik and Helmut Eschrig, “Full-potential nonorthogonal local-orbital minimum-basis band-structure scheme,” *Phys. Rev. B* **59**, 1743–1757 (1999).
- [45] MP Lopez Sancho, JM Lopez Sancho, JM Lopez Sancho, and J Rubio, “Highly convergent schemes for the calculation of bulk and surface green functions,” *Journal of Physics F: Metal Physics* **15**, 851 (1985).
- [46] R Bendorius, VD Prochukhan, and A Šileika, “The lowest conduction band minima of a2b4c-type semiconductors,” *physica status solidi (b)* **53**, 745–752 (1972).
- [47] J. L. Shay, B. Tell, E. Buehler, and J. H. Wernick, “Band structure of zngep₂ and zn₂sp₂ — ternary compounds with pseudodirect energy gaps,” *Phys. Rev. Lett.* **30**, 983–986 (1973).
- [48] F. Chiker, B. Abbar, S. Bresson, B. Khelifa, C. Mathieu, and A. Tadjer, “The reflectivity spectra of zn_xpn₂ (x=si, ge, and sn) compounds,” *Journal of Solid State Chemistry* **177**, 3859–3867 (2004).
- [49] SR Zhang, LH Xie, SD Ouyang, XW Chen, and KH Song, “Electronic structure, chemical bonding and optical properties of the nonlinear optical crystal zngep₂ by first-principles calculations,” *Physica Scripta* **91**,

- 015801 (2015).
- [50] V. N. Brudnyi, V. G. Voevodin, and S. N. Grinyaev, “Deep levels of intrinsic point defects and the nature of “anomalous” optical absorption in zngep2,” *Physics of the Solid State* **48**, 2069–2083 (2006).
- [51] Wolfgang Kraut and Ralph von Baltz, “Anomalous bulk photovoltaic effect in ferroelectrics: A quadratic response theory,” *Phys. Rev. B* **19**, 1548–1554 (1979).
- [52] Ralph von Baltz and Wolfgang Kraut, “Theory of the bulk photovoltaic effect in pure crystals,” *Phys. Rev. B* **23**, 5590–5596 (1981).

VI. APPENDIX

Figure 4 represents the orbital projected partial density of states for different atoms for ZnGeP_2 . Figure 5(a)-(h) show the calculated bulk 3D Fermi surface distribution in full Brillouin zone for different chemical potentials $E_f = 1.33, 1.43, 1.52, 1.68, 2.1, 2.11, 2.13, 2.15$ eV re-

spectively.

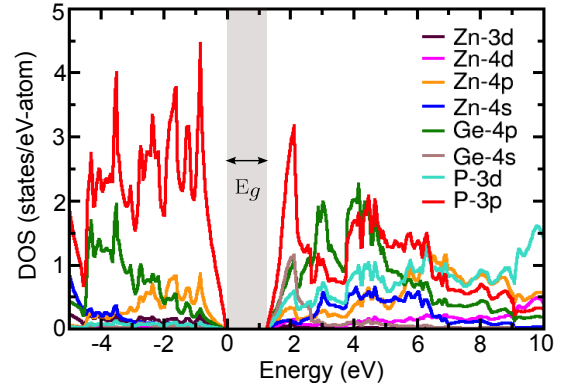


FIG. 4. Orbital projected partial density of states for different atoms in ZnGeP_2 .

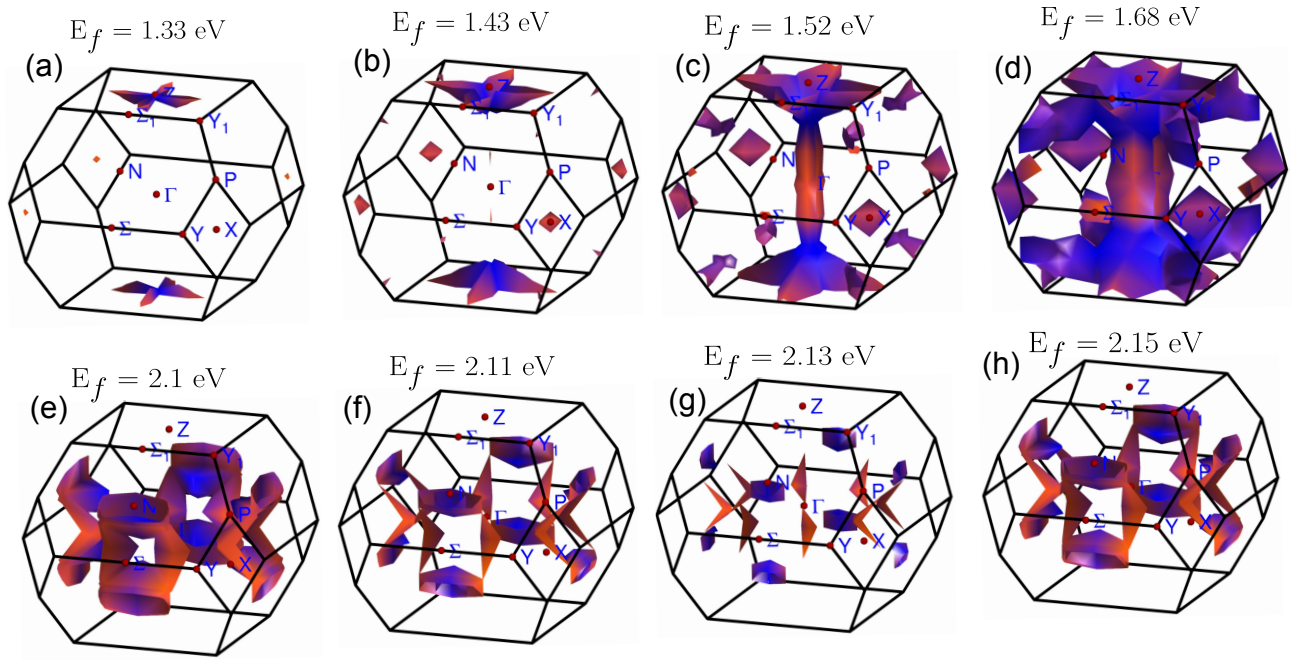


FIG. 5. (a)-(h) Calculated 3D Fermi surface for ZnGeP_2 in full Brillouin zone with different chemical potentials E_f .